Enhancing Intracellular Concentration and Target Engagement of PROTACs with Reversible Covalent Chemistry

Wen-Hao Guo,[1,†] Xiaoli Qi,[1,†] Yang Liu,[2] Chan-I Chung,[3] Fang Bai,[4] Xingcheng Lin,[5] Dong Lu,[1] Lingfei Wang,[1] Jianwei Chen,[1] Krystle J. Nomie,[2] Feng Li,[6,7] Meng C. Wang,[8,9,10] Xiaokun Shu,[3] José N. Onuchic,[4] Jennifer A. Woyach,[11] Michael L. Wang,[2] and Jin Wang[1,7,12*]

1. Department of Pharmacology and Chemical Biology, Baylor College of Medicine, Houston TX 77030, USA.

2. Department of Lymphoma/Myeloma, Division of Cancer Medicine, The University of Texas MD Anderson Cancer Center, Houston, TX 77030, USA.

3. Department of Pharmaceutical Chemistry, University of California−San Francisco, San Francisco, CA 94158, USA.

4. Center for Theoretical Biological Physics, Rice University, Houston, TX 77005, USA.

5. Department of Chemistry, Massachusetts Institute of Technology, Cambridge, MA 02139, USA.

6. Department of Pathology and Immunology, Baylor College of Medicine, Houston TX 77030, USA.

7. Center for Drug Discovery, Baylor College of Medicine, Houston TX 77030, USA.

8. Department of Molecular and Human Genetics, Baylor College of Medicine, Houston TX 77030, USA.

9. Huffington Center on Aging, Baylor College of Medicine, Houston, TX 77030, USA.

10. Howard Hughes Medical Institute, Baylor College of Medicine, Houston, TX 77030, USA.

11. Department of Internal Medicine, Division of Hematology, The Ohio State University, Columbus, OH 43210.

12. Department of Molecular and Cellular Biology, Baylor College of Medicine, Houston TX 77030, USA.

† Contributed equally

* Corresponding email: wangj@bcm.edu

Abstract

Current efforts in the proteolysis targeting chimera (PROTAC) field mostly focus on choosing the appropriate E3 ligase for a certain targeted protein, improving the binding affinities towards the target protein and the E3 ligase, and optimizing the PROTAC linker. However, it is well known that due to the large sizes of PROTAC molecules, their cellular uptake level remains an issue, posing a challenge to translate PROTACs into therapeutics. Driven by our fundamental investigation to compare how different warhead chemistry, reversible noncovalent (RNC), reversible covalent (RC), and irreversible covalent (IRC) binders, may affect the degradation of a model protein Bruton's Tyrosine Kinase (BTK), we serendipitously discovered that cyano-acrylamide-based reversible covalent chemistry can significantly enhance the intracellular concentration and target engagement of the PROTAC. Building on this discovery, we developed RC-1 as the first reversible covalent BTK PROTAC, which has high target occupancy and is effective as both an inhibitor and a degrader. Molecular dynamics calculations and phase-separation based ternary complex assays support that RC-1 forms a stable ternary complex with BTK and Cereblon (CRBN). Additionally, RC-1 compares favorably with other reported BTK degraders in cell viability and target engagement assays and has a reasonable plasma half-life for *in vivo* applications. Importantly, this reversible covalent strategy can be generalized and applied to improve other PROTACs. This work can not only help to develop optimal BTK degraders for clinical applications but also provide a new strategy to improve PROTAC efficacy.

Introduction

A proteolysis targeting chimera (PROTAC) is a heterobifunctional molecule that can bind both a targeted protein and an E3 ubiquitin ligase to facilitate the formation of a ternary complex, leading to ubiquitination and ultimate degradation of the target protein [1]. Since Crews and Deshaies conceived the PROTAC concept in 2001 [2], PROTACs have gained tremendous attention in recent years not only for their numerous applications in chemical biology but also as highly promising therapeutic agents [1]. Compared with oligonucleotide and CRISPR therapeutics that face *in vivo* delivery challenges, PROTACs are small molecule therapeutics that provide opportunities to achieve broadly applicable body-wide protein knockdown. ARV-110, an oral androgen receptor (AR) protein degrader, is the first PROTAC hitting the clinic in 2019 [3].

Protein degraders have many advantages compared with traditional small molecule inhibitors. First, small molecule inhibitors usually modulate protein functions through stoichiometrically occupying the active sites or binding pockets of targeted proteins; however, PROTACs act as catalysts and are involved in multiple cycles of targeted protein degradation [4,5]. Therefore, the degradation induced by PROTACs is sub-stoichiometric. Second, due to the competitive nature of small molecule inhibitors, constant systemic drug exposure is necessary to maintain sufficient intracellular concentrations for therapeutic efficacy, usually leading to off-target and side effects. In contrast, optimized PROTACs usually achieve maximal protein degradation in a few hours and maintain the therapeutic effect (even without constant PROTAC exposure) until the targeted protein is re-synthesized in cells. Therefore, the pharmacodynamics (PD) of PROTACs is dependent on not only drug exposure (pharmacokinetic (PK) properties) but also the half-life ($t_{1/2}$) of the targeted protein. Third, small molecules usually interfere with the function of one domain of a multidomain protein. However, this strategy for multidomain kinases, especially in cancer cells, may lead to compensatory feedback activation of its downstream signaling pathways *via* other alternative kinases [6]. In contrast, although PROTACs only target one domain of a multidomain protein, they induce degradation of the full-length protein, reducing the possibility to develop drug resistance through mutations or compensatory protein overexpression and accumulation [7]. Fourth, the specificity of small molecule inhibitors depends solely on the molecular design, which is sometimes difficult to achieve due to the presence of proteins with similar binding pockets, such as kinases. In contrast, the specificity of PROTACs is determined by not only the small molecule binder to targeted proteins but also the protein-protein interactions between the targeted protein and the recruited E3 ligase [8-11]. Last but not least, the targets of small molecular

inhibitors are usually enzymes and receptors with defined binding pockets or active sites. However, ~75% of the human proteome lacks active sites, such as transcription factors and non-enzymatic proteins, and are considered 'undruggable' [1]. In contrast, PROTACs can be designed to bind to any crevice on the surface of the targeted proteins to induce their degradation [12].

Most, if not all, PROTACs reported thus far have been based on noncovalent binding to their target proteins. Although irreversible covalent inhibitors, such as ibrutinib, have achieved tremendous clinical success based on their strong target affinities and high target occupancies, it was recently reported that PROTACs with irreversible covalent binders to targeted proteins failed to induce efficient protein degradation [13]. Although the potential mechanism accounting for the inhibition of protein degradation was not elucidated, it was postulated that irreversible covalent PROTACs are unable to induce protein degradation in a sub-stoichiometric/catalytic manner because they are consumed once they bind to their targeted protein. However, there are also examples arguing against this hypothesis [5,14].

Reversible covalent chemistry previously enabled our development of a series of fluorescent probes that can quantify glutathione concentrations in living cells [15-19]. We were curious whether reversible covalent PROTACs can not only enhance the binding affinity to targeted protein but also overcome the "one-shot deal" drawback of irreversible covalent PROTACs (**Figure 1**). Beginning as a basic science exploration to compare how the warhead chemistry of PROTACs affect protein degradation, we chose Bruton's tyrosine kinase (BTK) as a model target to test the hypothesis. To our surprise, we discovered that cyano-acrylamide-based reversible covalent binder to BTK can not only significantly enhance drug uptake in cells but also form stable ternary complexes by reducing protein conformational flexibility, compared with the non-covalent PRTOAC counterparts. Additionally, we found that this reversible covalent strategy can be generalized and applied to improve other PROTACs. We hope that this study can add another dimension to improve the cellular efficacy of PROTACs.

Results

Comparison of Different PROTAC Warhead Chemistry for BTK Degradation

As the first FDA-approved covalent kinase inhibitor, Ibrutinib irreversibly reacts with the free cysteine residue (C481) in the active site of BTK to form a covalent bond. It is also known that ibrutinib can still bind to the C481S BTK mutant mostly through hydrogen bonding, but with >40 folds lower affinity [20]. Johnson et al. showed that

ibrutinib is >6 folds more potent than its Michael acceptor saturated ibrutinib analog in a kinase inhibition assay for wild type BTK (IC_{50} 0.72 nM vs 4.9 nM), while both compounds are equally potent towards BTK C481S mutant (IC_{50} 4.6 nM vs 4.7 nM) [21]. To compare how different warhead chemistry may affect the target protein degradation, we designed three PROTAC molecules, RC-1, RNC-1 and IRC-1, which form reversible covalent (RC), reversible noncovalent (RNC), and irreversible covalent (IRC) binding to BTK (**Figure 2A**). Following previous work [13,22-26], we chose pomalidomide as the CRBN E3 ligase binder. RC-1, RNC-1 and IRC-1 share the same linker and E3 ligand binder and differ only by the binding moieties to BTK. We chose MOLM-14, an acute myeloid leukemia cell line, as a model system to study PROTAC-mediated BTK degradation following previous work [23].

To test whether the three PROTACs can induce BTK degradation, we treated MOLM-14 cells with RC-1, RNC-1 and IRC-1 for 24 h, followed by Western blot to quantify the total BTK levels (**Figure 2B**). We found that IRC-1 induced minimal BTK degradation even at 1 μM, the highest concentration used in this study, while RNC-1 reduced the BTK level by ~50% at 200 nM, consistent with Tinworth et al.'s recent report [13]. Compared with RNC-1 and IRC-1, RC-1 potently induced BTK degradation in MOLM-14 cells (DC_{50} = 6.6 nM, **Figure 2C**), as one of the most potent BTK degraders reported so far [13,24]. Additionally, neither the RC-1 warhead, nor pomalidomide, nor a combination of both caused BTK degradation (**Figure 2D**), indicating that the bifunctional PROTAC molecule is essential to facilitate the formation of a ternary complex of {BTK-PROTAC-CRBN} to induce BTK degradation.

Linker Optimization for Reversible Covalent BTK PROTAC

Encouraged by the promising result for RC-1, we set out to optimize the linker between the BTK covalent reversible binder and pomalidomide (**Figure 3**). In a recent study from Pfizer, Zorba et al. showed that increasing PROTAC linker length alleviates steric clashes between BTK and CRBN and improves the efficacy of BTK degradation [24], indicating the absence of thermodynamic cooperativity in the formation of a ternary complex of {BTK-PROTAC-CRBN}. Therefore, we synthesized RC-2, RC-3, RC-4 and RC-5, which are 1, 2, 5, and 8 atoms longer in the linker length compared with RC-1. Contrary to Pfizer's finding, we found that RC-1 is the most efficacious for BTK degradation compared with the PROTACs possessing longer linkers, suggesting cooperative ternary complex formation (**Figure S1**).

To test whether the BTK degradation efficacy of RC-1 can be improved through further reducing the linker length, we designed RC-6, RC-7 and RC-8, which are 1, 2, and 3 atoms shorter in the linker length compared with RC-1. Unfortunately, we could not synthesize RC-6 due to an intramolecular reaction between the amide and the Michael acceptor. Comparing the BTK degradation capability in MOLM-14 cells, we found that RC-7 and RC-8 are inferior to RC-1, possibly due to unfavorable steric clashes between BTK and CRBN. We also found that the efficacy of BTK degradation decreases significantly through only a single atom change of the thalidomide aryl amine nitrogen to an oxygen (RC-9) (**Figure S1**).

In Buhimschi et al.'s recent study, a BTK PROTAC MT-802 has the linker placed at the C5 position on the phthalimide ring of pomalidomide instead of the C4 position as in RC-1. We synthesized RC-10 by placing the linker at the C5 position of the phthalimide ring and found that RC-10 cannot induce any BTK degradation (**Figure S1**). Therefore, we concluded that RC-1 has the optimal linker length and position for BTK degradation with the BTK and CRBN binders used.

Quantitative Measurements of BTK and CRBN Concentrations in Cells

The Crews group developed a series of PROTACs for TANK-Binding Kinase 1 (TBK-1) with different binding affinities towards TBK-1 and von Hippel-Lindau (VHL), the E3 ligase recruited [27]. We re-analyzed the data in this study and found a strong correlation between binding affinities towards TBK-1 and the DC_{50} values in cells (**Figure S2**), suggesting that tighter binding to the target protein leads to more efficient PROTAC-induced protein degradation in cells. In our study, it is reasonable to assume that the binding affinity of RC-1 to BTK is higher than RNC-1 due to the covalent bond formed between RC-1 and BTK. It could be taken for granted that tighter binding to BTK leads to more formation of the ternary complex, resulting in more efficient BTK degradation. However, the formation of the {BTK-PROTAC-CRBN} ternary complex depends on not only the binding affinities of PROTAC towards BTK and CRBN but also the **absolute concentrations** of BTK, CRBN and PROTAC in cells. To the best of our knowledge, previous studies on PROTACs only focus on the biochemical measurements for binding affinities of PROTACs to target proteins and E3 ligases without knowing the intracellular concentrations of these proteins.

We performed quantitative Western blots to measure the levels of BTK and CRBN in MOLM-14 cells using a series of concentrations of their corresponding recombinant proteins as the standards. Lysate from a million

MOLM-14 cells usually produces 250 μg of protein as determined by BCA assays. Because proteins usually occupy 20-30% of cell volume (assuming 25% w/v, i.e., 250 mg/mL) [28], we can calculate the volume of 1 million MOLM-14 cells to be ~1 μL (i.e., the volume of each MOLM-14 cell is ~1000 μm^3). Based on quantitative Western blots, we determined the total amount of BTK and CRBN in 1 million MOLM-14 cells to be 60 and 0.72 ng, respectively. Considering the molecular weights of BTK and CRBN are 77 kD and 55 kD, we can deduce the absolute concentrations for BTK and CRBN in MOLM-14 cells are 780 and 13 nM, respectively (**Figure 4A and Figure S3**). Based on our biochemical binding assays, the *K*d values between PROTACs and BTK are in the range of 3.0–6.4 nM (**Table 1**), while the *K*d values between the PROTACs and CRBN are in the range of 1.5–4.2 μM (**Table 2**). Assuming there is no cooperativity effect in the formation of the ternary complex {BTK-PROTAC-CRBN}, we can predict that BTK PROTACs binding to CRBN is the determining factor for ternary complex formation due to the low abundance of CRBN and the weak binding between pomalidomide and CRBN. Therefore, under this situation, further increasing PROTAC binding affinities to BTK, such as comparing RC-1 and RNC-1, would not lead to a meaningful increase of ternary complex formation. This conclusion is also supported by the mathematical model for three-body binding equilibria developed by Douglass et al. [29] (**Figure S4**).

Imaging of Ternary Complex Formation in Live Cells

To visualize small molecule-induced protein-protein interaction (PPI), recently we applied fluorophore phase transition-based principle and designed a PPI assay named SPPIER (separation of phases-based protein interaction reporter) [30]. SPPIER includes two proteins of interest, an enhanced GFP (EGFP) and two homo-oligomeric tags (HOTag). Upon small molecule-induced PPI between two proteins of interest, multivalent (from HOTag) PPI drives EGFP phase separation, forming brightly fluorescent droplets. Here, to detect PROTAC-induced PPI between cereblon (CRBN) and BTK, we engineered the kinase domain of BTK (amino acid residues 382 – 659, referred to as BTK^{KD}) into SPPIER (**Figure 5A**). This assay is named BTK-SPPIER, which includes two constructs: BTK^{KD}-EGFP-HOTag6 and CRBN-EGFP-HOTag3. HEK293 cells were transiently transfected with both constructs. Twenty-four hours after transfection, the cells were incubated with 10 μM of RC-1, IRC-1 or RNC-1. Live cell fluorescence imaging revealed that RC-1, but not IRC-1 nor RNC-1, induced green fluorescent droplets (**Figure 5B**). This imaging result indicated that RC-1 promoted multivalent PPI and formation of ternary complex formation among RC-1, BTK^{KD} and, CRBN. This data demonstrates that RC-1 is more efficient

to induce ternary complex formation than RNC-1 and IRC-1 in living cells. It should be noted that the concentration needed for RC-1 to induce appreciable droplet formation in this assay is much higher than its DC_{50} in MOLM-14 cells potentially due to the high overexpression of the target proteins and the sensitivities of the assay.

Inhibition of Cell Viabilities by BTK Degraders

We next examined the potencies of inhibiting cell growth for RC-1, IRC-1, RNC-1, RC-1-Me (RC-1 non-degrader control), and their corresponding BTK binder controls, RC-Ctrl, IRC-Ctrl (i.e. ibrutinib), and RNC-Ctrl in MOLM-14 cells. All the chemical structures and IC_{50} values can be found in **Figure 2A** and **Table 1,** respectively. Differing by a methyl group, RC-1 can but RC-1-Me cannot degrade BTK in cells (**Figure 2D**). Interestingly, both compounds have similar IC_{50} values (0.31 vs 0.21 μM), suggesting that BTK inhibition but not degradation accounts for the toxicity in MOLM-14 cells. The IC_{50} values for RC-Ctrl, IRC-Ctrl, and RNC-Ctrl are also similar in the range of 0.3–0.5 μM, suggesting that these three warheads inhibit BTK to a similar extent in cells. Surprisingly, both the IC_{50} values for IRC-1 and RNC-1 are in the μM range (2.7 and 4.1 μM). A biochemical BTK kinase inhibition assay showed that IRC-1 and RNC-1 have slightly diminished inhibitory activities (< 3-fold) compared with their corresponding warhead controls (**Table 1**). However, the difference between enzymatic activities is insufficient to explain the >10-fold difference in IC_{50} values in cells, suggesting that IRC-1 and RNC-1 may have poorer cellular permeability than their corresponding warhead controls. In contrast, RC-1 and RC-Ctrl have similar IC_{50} values in both biochemical BTK inhibition and cellular growth inhibition assays (**Table 1**), suggesting similar compound exposure in cells. The growth inhibition assay for the BTK degraders prompted us to investigate alternative mechanisms to explain the high potency of RC-1.

Comparison of Intracellular Concentrations of BTK Degraders

Since the binding affinities between BTK and its PROTACs cannot explain the difference in BTK degradation between RC-1 and RNC-1 and potencies for cell growth inhibition among RC-1, RNC-1 and IRC-1, we asked whether the intracellular concentration of RC-1 may be higher than those of RNC-1 and IRC-1, leading to more potent pharmacological effects. To test this possibility, we turned to the Nano-luciferase based bioluminescence resonance energy transfer (NanoBRET) assay developed by Promega [31]. HEK-293 cells were transiently transfected with plasmids expressing a fusion protein of Cereblon and nano-luciferase (nLuc) for 24 h and then

the cells were treated with a Cereblon tracer, which binds to Cereblon to induce NanoBRET signals. Adding PROTACs to cells would compete the CRBN tracer binding to CRBN, thus reducing the NanoBRET signals. It should be noted that the NanoBRET assay is ratiometric and independent of the expression level of the nLuc fusion protein. Based on this assay, we found that the CRBN target engagement IC_{50} value of RC-1 is 3- and 9-fold lower than those of IRC-1 and RNC-1, respectively (**Figure 4B**). Combining the in-cell target engagement IC_{50} and K_d to CRBN (**Table 2**), we can deduce that the intracellular concentration of RC-1 is 9 and 22 folds higher than those of IRC-1 and RNC-1, respectively. Additionally, the calculated CLogP and polar surface area (PSA) values for these three compounds are similar (**Table S1**), arguing against the possibility that the physicochemical properties of RC-1 are the cause of its high intracellular concentration. The high cellular uptake of RC-1 might be due to its reversible covalent interactions with cell surface thiols [32,33]. Therefore, we conclude that the efficient BTK degradation and potent cell growth inhibition induced by RC-1 is achieved mostly through its high intracellular concentration, due to the reversible covalent structural moiety in RC-1.

RC-1 is a unique BTK degrader with high target occupancy

Although the PROTACs are characterized as BTK degraders, they have warheads that can bind and inhibit BTK, essentially as dual-functional BTK inhibitors and degraders. We performed biochemical BTK kinase inhibition assays to measure the IC_{50} values for RC-1, RNC-1 and IRC-1 and their corresponding warhead controls (**Table 1** and **Figure S5**). IRC-Ctrl (i.e. Ibrutinib) forms a covalent bond with BTK and is expected to be the most potent BTK inhibitor (IC_{50} = 0.3 nM). In comparison, RC-Ctrl and RNC-Ctrl have reduced BTK inhibition activities by 7 and 45 folds, respectively. The BTK PROTACs, RC-1, RNC-1, and IRC-1, have similar BTK inhibitory activities to their corresponding warheads (**Table 1 and Figure S5**).

We then performed a similar NanoBRET based live-cell target engagement assay for BTK. Consistent with the CRBN target engagement assay, we found that the BTK target engagement IC_{50} value of RC-1 is 3 and 26 folds of the values for IRC-1 and RNC-1, respectively (**Figure 4C**). Combined the in-cell target engagement IC_{50} and K_d to BTK (**Table 1**), we can deduce that the intracellular concentration of RC-1 is 6 and 35 folds higher than those of IRC-1 and RNC-1, respectively, similar to the trend observed in the CRBN target engagement assay (**Figure 4B**).

Due to poor permeability, most PROTACs have low target occupancy (**Figure 4D**) and rely on the sub-stoichiometric protein degradation to achieve maximal efficacy. Using the NanoBRET-based BTK in-cell target engagement assay, we found that RC-1 can achieve 50% and 90% of target engagements at 40 and 200 nM, respectively. Therefore, RC-1 can function as both a BTK inhibitor and degrader.

RC-1 degrades BTK regardless of its mutation status

Mutations in BTK, C481S in particular, confer ibrutinib resistance in clinic [20]. We set out to test whether BTK degradation induced by our PROTACs is affected by BTK mutation status. XLA cells overexpressing wild type BTK or C481S mutant BTK were treated with RC-1, RNC-1 and IRC-1 for 24 h, followed by Western blot to compare the BTK levels (**Figure 6A and Figure S6**). We observed dose-dependent BTK degradation induced by RC-1 regardless of its mutation status with comparable potency. This observation is consistent with our previous conclusion that altering PROTAC binding affinities to BTK within a range does not significantly change the ternary complex formation efficiency (**Figure S4**). It should be noted that the potency of RC-1 is weaker in XLA cells than in MOLM-14 cells possibly because BTK is overexpressed in XLA cells. It is also interesting to note that IRC-1 induces much more effective degradation of the BTK C481S mutant than its wild type in XLA cells (**Figure S6**), suggesting that the irreversible covalent bond formation between IRC-1 and BTK causes the inefficient protein degradation, consistent with the previous study by the GSK group [13].

RC-1 degrades BTK with higher specificity than IRC-1 and RNC-1

To explore the effects of our degraders on the whole proteome, we treated MOLM-14 cells with RC-1, RNC-1, IRC-1, RC-1-Me (non-degrader control) or DMSO and employed a quantitative multiplexed proteomic approach to measure the whole cellular protein levels (**Figure 7**). The result showed that both in IRC-1 and RNC-1-treated cells, 7 kinases are degraded including BTK. However, for RC-1-treated cells, only 2 kinases (BTK and CSK) can be degraded, suggesting that RC-1 has more selectivity than IRC-1 and RNC-1 for kinase degradation. However, no degradation is observed in RC-1-Me-treated cells, indicating that this degradation is CRBN dependent. In addition, immunomodulatory imide drugs (IMiD)-dependent substrates including IKZF1, ZFP91 and ZNF692 are also specifically degraded by RC-1, RNC-1 and IRC-1.

Molecular dynamics simulations predict a stable ternary complex for RC-1

To better understand the ternary complex formation, we applied molecular dynamics simulations to evaluate the global rearrangement of the ternary structures for BTK, CRBN, and RC-1 or IRC-1 or RNC-1, and compared the binding stabilities of these three ligands to BTK and CRBN. The residue-based RMSF (root mean square fluctuations) was calculated based on the entire simulation trajectory (>200 ns) to assess the average fluctuation of each residue of the three simulated complexes. It is clear that RNC-1 mediated complex {BTK-RNC-1-CRBN} has the largest fluctuation compared with the other two complexes {BTK-RC-1-CRBN} and {BTK-IRC-1-CRBN} (**Figure 8A**), suggesting that covalent binding could help to overcome the unfavorable entropy penalties during the ternary complex formation. Additionally, the RMSD (Root-mean-square deviation) values were calculated based on the Cα atoms to reflect the conformation changes from the input structures based on x-ray crystallography. Consistent with the RMSF analyses, the RMSD changes for the {BTK-RC-1-CRBN} and {BTK-IRC-1-CRBN} complexes are much smaller than the one for the {BTK-RNC-1-CRBN} complex, suggesting that covalent bonding can help to stabilize the ternary complexes (**Figure 8B**).

Low energy conformations of the protein complex can shed light on the detailed molecular interactions which stabilize the binding interface. The conformation with the lowest energy along the trajectories was extracted and shown in **Figure 8C**. The binding mode and critical molecular interactions, i.e., hydrogen bonds and π-π interactions formed between the ligands and BTK and CRBN, are conserved compared to the crystal structure of BTK/ibrutinib and CRBN/lenalidomide. From the predicted binding mode, several hydrogen bonds and the covalent bond between RC-1 and the residue C481 of BTK anchors the ligand to the binding site of BTK. Additionally, a hydrogen bond between Y355 of CRBN and anion-π interaction formed between H353, hence, further greatly stabilizes the binding of RC-1 with proteins, and help to hold the orientation of RC-1 to adjust and stabilize the ternary complexes (**Figure 8C**).

RC-1 outperforms other reported BTK degraders in Cell Viability and Target Engagement Assays

The goal of blocking BTK signaling with either BTK inhibitors or degraders is to inhibit the growth of cancer cells. To this end, we synthesized the BTK degraders reported by Pfizer (compound 9) [24], the Gray group (DD-03-171) [26], and the Crews' group (MT-802) [25] and compared them head-to-head with RC-1, RNC-1 and IRC-1 in their abilities to inhibit cancer cell growth (**Figure 9 and Figure S7**). Due to the structural similarities of RNC-1 and the BTK degraders reported by the GSK group (PROTAC 5) [13] and the Rao group [22], we used RNC-1 as a

surrogate for comparison. In MOLM-14 cells, RC-1 has the most potent inhibitory effect among all the PROTACs compared (**Figure 9 and Figure S7**). It is interesting to note that RC-1 and RC-1-Me, which does not induce BTK degradation, have similar IC_{50} values in inhibiting MOLM-14 cell growth, indicating that the growth inhibitory effect induced by PROTACs in MOLM-14 cells is due to BTK inhibition instead of its degradation. The high potency of RC-1 is possibly due to the combinatorial effects of its high intracellular concentration and tight binding to BTK.

We also compared the potency of BTK degraders in Mino cells, a BTK dependent MCL cell line. In Mino cells, RC-1 and Gray's BTK degrader have comparable potency for inhibiting cell growth and outperform all the other BTK PROTACs tested (**Figure 9B**). Additionally, RC-1 can degrade not only BTK and phosphorylated BTK but also IKZF1 and IKZF3 (**Figure 6C**), similar to Gray's BTK degrader [26]. It is interesting to note that RC-1 is more potent than ibrutinib in Mino cells, but have similar potencies in Jeko-1, Rec-1 and Maver-1 cells (**Figure 6B**). Further investigation is required to identify biomarkers for the subtype of MCL sensitive to BTK degraders.

Additionally, we compared BTK in-cell target engagement among RC-1, RC-Ctrl (RC-1 warhead) and these reported BTK degraders (**Figure 4D**). It is remarkable to see that the target engagement IC_{50} values for RC-1 and RC-Ctrl (63 vs 67 nM) are the same within experimental errors, demonstrating that the cellular permeability of RC-1 is essentially the same as its parent warhead molecule although their molecular weights differ by 1.7 folds. In contrast, the target engagement IC_{50} values for Gray's and Crews' BTK degraders are 4 and 10 folds of that of RC-1, respectively. Surprisingly, Pfizer's BTK degrader did not show appreciable target engagement even at 10 μM.

RC-1 has an ideal plasma half-life and degrades BTK in vivo

We measured the plasma half-life of RC-1 (20 mg/kg, i.p. injection) in ICR mice (female, 5-6 weeks, n=3) using LC-MS/MS. The PK data were fitted into a non-compartmental model using PK solver [34]. RC-1 has a plasma half-life ($t_{1/2}$) of 3.4 h, C_{max} of 20 μM, and AUC of 72 μM·h (**Figure 10A**). To further test the pharmacodynamics of RC-1 *in vivo*, we treated ICR mice (n=3) with 20 mg/kg of RC-1 (i.p. injection). After 7 days injection, the mice were sacrificed, and their spleens, the locations of the majority of B cells, were collected. Western blotting showed that RC-1-treated mice had ~50% BTK level reduction in the spleens compared with the DMSO-treated mice (**Figure 10B**). Therefore, this preliminary study showed that RC-1 has desirable PK/PD

properties *in vivo*, laying the foundation for future efficacy tests in mouse models to ultimately move this degrader into the clinic.

Other reversible covalent PROTACs with improved target engagement

Based on the success of RC-1, we were curious whether cyano-acrylamide based reversible covalent PROTACs can be generally applied to improve target engagement. An activating mutation of Fms-like tyrosine kinase 3 (FLT3) is the most frequent genetic alteration associated with poor prognosis in acute myeloid leukemia (AML). Similar to BTK, FLT3 also has a cysteine residue in the ATP binding pocket. Yamaura et al. reported a highly potent irreversible covalent FLT3 inhibitor, termed as FF-10101 [35]. Building on this work, we designed a series of reversible covalent, irreversible covalent and reversible non-covalent FLT3 PROTACs. Using the NanoBRET CRBN in-cell target engagement assay, we found that RC-FLT3 has a similar target engagement IC_{50} value compared with that for pomalidomide (**Figure 11**). Similar to BTK PROTACs, the target engagement IC_{50} values for IRC-FLT3 and RNC-FLT3 PROTACs are 6 and 47 folds of the value for RC-FLT3 (**Figure 11**). This experiment confirmed that introducing a cyano-acrylamide moiety can be a general strategy to enhance cellular permeability for PROTACs.

Discussion

Despite the exciting promise of PROTACs, the development of this type of therapeutic agent faces some major challenges. Due to the high molecular weights of PROTACs, they are not druglike based on the commonly applied empirical rules for drug discovery and tend to have poor membrane permeabilities, resulting in low drug concentrations inside cells. Therefore, PROTACs usually have low target occupancy and heavily depend on sub-stoichiometric protein degradation to achieve therapeutic efficacy. Although there are successful PROTAC examples with potent *in vitro* and *in vivo* efficacies, they are mostly optimized through “brute force” medicinal chemistry efforts. To the best of our knowledge, few efforts have been focused on developing general strategies to improve the cellular permeability of PROTACs. In this work, we serendipitously discovered that cyano-acrylamide groups can function as “molecular transporters” to improve the cellular permeability of PROTACs. Based on Taunton’s and our own previous work [16,19,36], it has been well established that cyano-acrylamides can reversibly react with thiols with mM dissociation equilibrium constants (K_d). Additionally, the reaction kinetics

between cyano-acrylamides and free thiols are fairly rapid. During the development of our GSH probe, we found that the RealThiol probe can establish equilibrium with GSH in 90 seconds in both forward and reverse reactions. There are many available free cysteine residuals on the cellular surface, which can reversibly react with cyano-acrylamide containing molecules to mediate the cellular uptake. The Matile group reported that strained cyclic disulfides can enhance cellular uptake of non-permeable molecules through a similar mechanism [32,33]. Although understanding the molecular mechanism of the potential thiol-mediated cellular uptake is out of the scope of this work, it would be interesting to explore other reversible covalent chemistry to enhance the cellular uptake of poorly permeable molecules.

The efficacy of irreversible covalent PROTACs has been controversial, with both successful [5,14] and unsuccessful examples [13]. An apparent drawback for irreversible covalent PROTACs is its non-catalytic degradation of target proteins. If we examine the target engagement data for IRC-1 (**Figure 4B and 4C**), it can achieve ~100% BTK and ~40% CRBN engagement at 400 nM of IRC-1. Assuming the target engagement IC_{50} values are similar in the HEK293 over-expression system and MOLM-14 cells, we would expect to observe significant BTK degradation with 400 nM of IRC-1 treatment, even with the single turnover degradation. However, very little BTK degradation was observed in MOLM-14 cells even with 1 μM of IRC-1 treatment, suggesting either BTK was not efficiently ubiquitinated due to the poor orientation of the ternary complex, or ubiquitinated BTK was not effectively degraded by proteasomes. The detailed mechanism to explain why IRC-1 cannot efficiently degrade BTK requires further investigations. Nonetheless, RC-1, the reversible covalent counterpart of IRC-1, addresses the non-catalytic degradation issue of IRC-1 and brings unexpected cellular permeability advantages.

Disrupting the kinase function of BTK using kinase inhibitors is the only currently available therapeutic intervention on this well-validated target. However, it was shown that BTK can enhance antigen receptor-induced calcium influx in a kinase-independent manner [37], while a kinase-inactive BTK mutant can partially rescue B cell development of *BTK* null B cells in mice [38]. Additionally, conditional mouse knockouts of *BTK* after the establishment of B-cell populations have shown that B-cell populations were maintained in conditional knockout mice [39], suggesting that BTK may not be essential for the survival of mature, normal human B-cells. This work supports the hypothesis that BTK degradation will have little effect on normal human B-cells, but will result in the cell death of MCL and CLL cells, which rely on BTK for survival and proliferation. In this work, we developed a small molecule therapeutic agent that can efficiently inhibit and degrade BTK irrespective of *BTK* mutation status

to abolish both BTK kinase and non-kinase activities completely**.** It should be noted that although a few BTK degraders have been reported [13,22,24-26], they all have low target engagement due to their poor cellular permeability (**Figure 4D**). It is usually very difficult for degraders to achieve 100% degradation of the target protein, and the remaining small portion of undegraded BTK can be sufficient to sustain the signaling cascades due to its enzymatic nature. Clinically, it is important for ibrutinib to achieve 100% BTK engagement to completely shut down the BTK downstream signaling. Our BTK degrader RC-1 is unique compared with other BTK degraders because it not only degrades BTK efficiently but also shows high target engagement to inhibit BTK in case BTK is not completely degraded. This novel dual mechanism of action (MOA) for BTK inhibition and degradation has never been explored in the clinic.

While we are submitting the manuscript, the London group published a preprint comparing the reversible covalent, irreversible covalent and reversible noncovalent BTK degraders [40]. In their study, the reversible covalent BTK PROTAC was not very potent in protein degradation assays compared with the irreversible covalent and reversible noncovalent counterparts. The main difference between our reversible covalent PROTAC and theirs is the dimethyl group at the γ-position of the cyanoacrylamide group in RC-1, which reduces the reactivity of the Michael acceptor, leading a mM K_d when reacting with small molecule thiols. The cyanoacrylamide in London's reversible covalent PROTACs is too reactive towards small molecule thiols. We speculate that due to the high reactivity of London's reversible covalent PROTACs, they may react with cysteine in the medium even before entering cells, thus reducing the intracellular concentration of the PROTACs. It would be interesting to compare London's and our BTK PROTACs in the same target engagement assay.

In summary, we have not only developed a unique dual-functional BTK inhibitor and degrader but also provided a general strategy to improve cellular permeability of PROTACs and other small molecules with poor cellular permeability. We are the first to apply reversible covalent chemistry to develop PROTACs and serendipitously discovered that the reversible covalent cyano-acrylamide moiety can function as a general molecular transporter to enhance intracellular accumulation of compounds. Our approach will address cellular permeability issues, a major problem of PROTAC development, and be generally applied to small molecule drugs with molecular weight > 500. Unlike other PROTACs with low target occupancy due to poor permeability, RC-1 has high target occupancy and is effective as both an inhibitor and a degrader. This feature is highly important to ensure undegraded BTK protein would still be inhibited by RC-1. Otherwise, the remaining small

portion of undegraded BTK can be sufficient to support its signaling cascades due to its catalytic nature. Additionally, molecular dynamics calculations and phase-separation based ternary complex assays also support that RC-1 forms a stable ternary complex with BTK and CRBN. Last but not least, RC-1 compares favorably with other reported BTK degraders in cell viability and target engagement assays and has a reasonable plasma half-life for *in vivo* applications. We hope this work can not only help to develop optimal BTK degraders for clinical applications but also provide a new strategy to improve PROTAC efficacy.

Conflict of Interests

J.W., W.G., X.Q., M.L.W., K.N., and Y.L. are the co-inventors of a patent related to this work. Additionally, J.W. is the co-founder of CoActigon Inc. and Chemical Biology Probes LLC.

Acknowledgment

The research was supported in part by Baylor College of Medicine seed funding to J.W. and Howard Hughes Medical Institute to M.C.W. Work at the Center for Theoretical Biological Physics sponsored by the NSF (Grants PHY-1427654 and CHE-1614101) and by the Welch Foundation (Grant C-1792). J.N.O. is a Cancer Prevention and Research Institute of Texas (CPRIT) Scholar in Cancer Research. We also thank Dr. Campos at SBP Medical Discovery Institute for his help with the proteomics experiment.

Table 1. BTK inhibition, In-Cell Target Engagement and Cell Viability

Compound	K_d (nM) [a]	BTK Inhibition IC_{50} (nM) [b]	Cell Viability IC_{50} (μM) [c]	BTK Target Engagement IC_{50} (μM) [d]	IC_{50}/K_d [e]
RC-1	6.4	1.8	0.31	0.039	6.1
IRC-1	3.0	0.8	2.7	0.11	37
RNC-1	4.7	21.2	4.1	1.0	213
RC-1-Me		6.8	0.21		
RC-Ctrl	9.1	2.2	0.50		
IRC-Ctrl		0.3	0.33		
RNC-Ctrl		13.6	0.42		

a. The dissociation equilibrium constant K_d was measured using the full-length BTK protein by Eurofins DiscoverX. The reported K_d values for RC-1, IRC-1 and RC-Ctrl were measured in the absence of DTT in the buffer. DTT (6 mM) used in the standard assay condition increases the K_d values of RC-1 and RC-ctrl by 2-3 folds, while it does not affect the measurement for IRC-1. The reported K_d value for RNC-1 was measured in the standard assay buffer with the presence of DTT. Duplicates were performed.

b. The biochemical BTK inhibition (BTK Inhibition IC_{50}) was measured using the BTK assay kit from AssayQuant Technologies Inc.

c. Cell viability IC_{50} was performed by treating MOLM-14 cells with compounds for 72 h, followed by Alamar Blue assay.

d. Target Engagement IC_{50} is the compound concentration required to achieve 50% BTK target engagement measured using a NanoBRET BTK in-cell target engagement assay. Triplicates were performed.

e. IC_{50}/K_d is normalized target engagement IC_{50} considering the difference for binding affinities between PROTACs and BTK.

Table 2. CRBN Binding and In-Cell Target Engagement

Compound	K_d (μM) [a]	IC_{50} (μM) [b]	IC_{50}/K_d [c]
RC-1	4.2	0.20	0.048
IRC-1	1.5	0.68	0.45
RNC-1	1.8	1.9	1.06
Pomalidomide	1.4		

a. The dissociation equilibrium constant K_d was measured using a truncated Cereblon protein. Triplicates were performed.

b. IC_{50} is the compound concentration required to achieve 50% CRBN target engagement measured using a NanoBRET CRBN in-cell target engagement assay. Triplicates were performed.

c. IC_{50}/K_d is normalized target engagement IC_{50} considering the difference for binding affinities between PROTACs and CRBN.

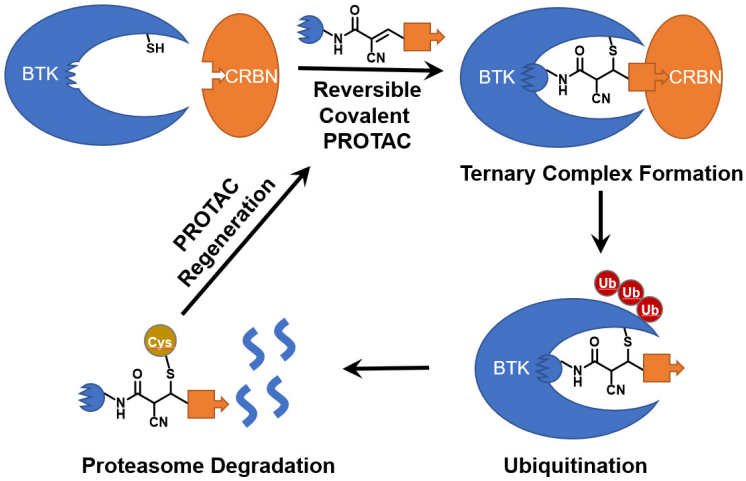

Figure 1. Demonstration of catalytic degradation of targeted proteins by reversible covalent PROTACs. The premise of this reversible covalent PROTAC design is the weak reactivity (mM K_d) between α-cyano-acrylamide group (the chemical structure shown above) and free thiols. Only when the PROTAC molecule binds to the active site of the targeted protein, the nearby cysteine side chain can react with the α-cyano-acrylamide group to form a stable covalent bond. Once the targeted protein is degraded, the reversible covalent PROTAC can be regenerated.

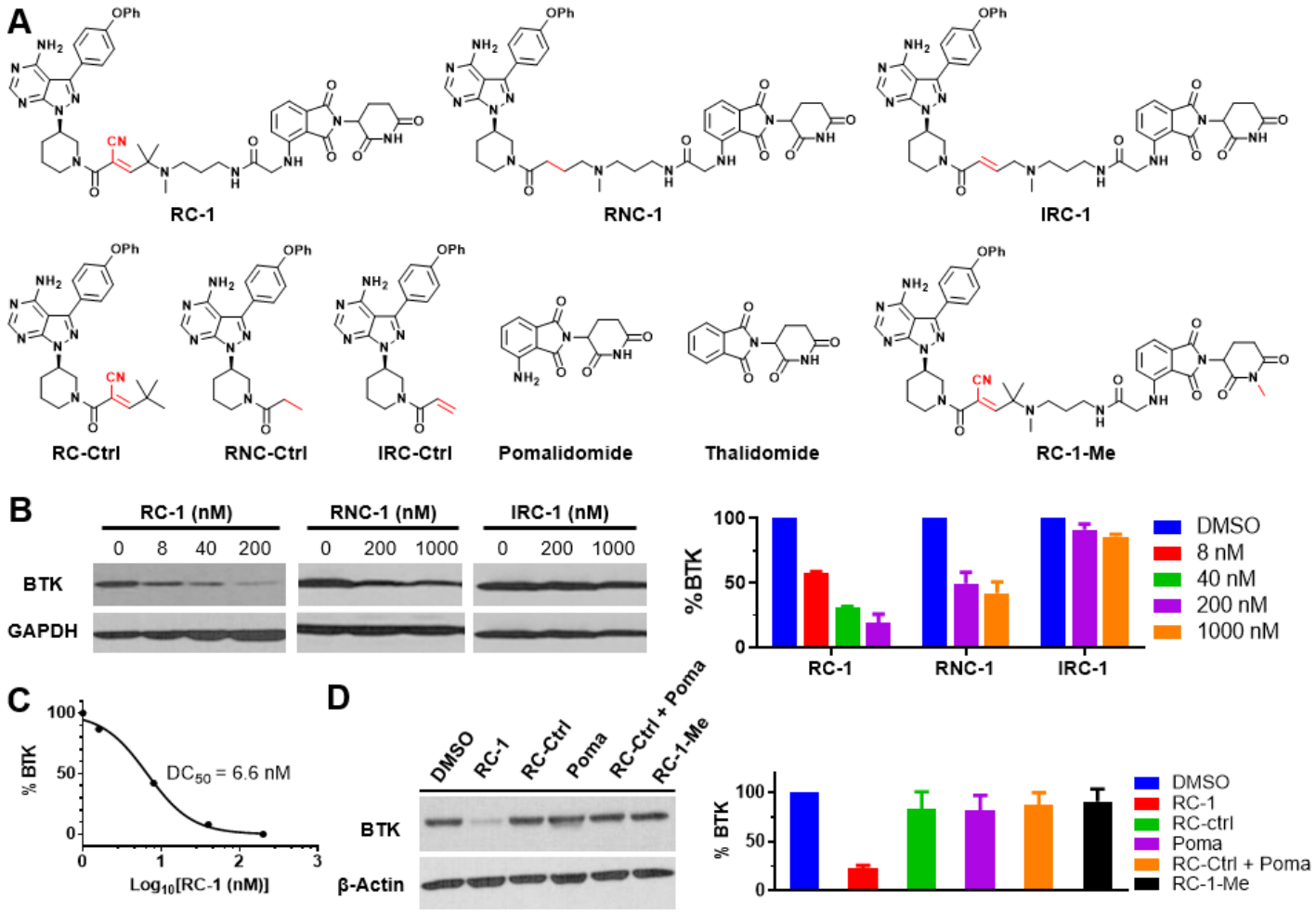

Figure 2. BTK degradation induced by PROTACs. (A) Chemical structures of BTK degraders and their controls. RC-1, RNC-1 and IRC-1 are BTK degraders with reversible covalent, reversible non-covalent, and irreversible covalent warheads, respectively. RC-Ctrl, RNC-Ctrl, and IRC-Ctrl (i.e., ibrutinib) are the corresponding warhead controls for RC-1, RNC-1 and IRC-1, respectively. (B) MOLM-14 cells were incubated with RC-1, RNC-1 and IRC-1 for 24 h. The BTK levels were quantified by Western blotting. Duplicates were performed. (C) RC-1 dose-dependent BTK degradation in MOLM-14 cells. DC_{50}: compound concentration inducing 50% of protein degradation. (D) MOLM-14 cells were treated with DMSO, RC-1, RC-Ctrl, Pomalidomide, RC-Ctrl + Pomalidomide, and RC-1-Me for 24 h. All the compound concentrations are 200 nM. Neither RC-Ctrl, nor pomalidomide, nor a combination of both caused BTK degradation, indicating that the bifunctional PROTAC molecule is essential to facilitate the formation of a ternary complex of {BTK-PROTAC-CRBN} in order to induce BTK degradation.

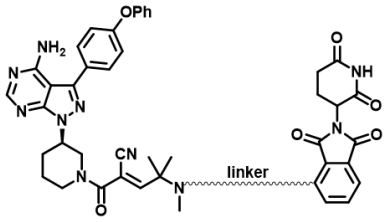

Compound	Linker	Degradation at 200 nM
RC-1	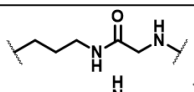	81%
RC-2	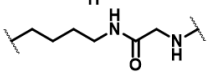	49%
RC-3	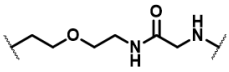	39%
RC-4	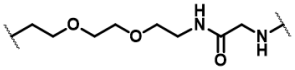	43%
RC-5	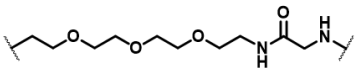	56%
RC-6	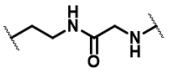	--
RC-7	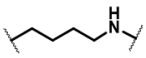	6%
RC-8	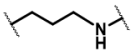	15%
RC-9	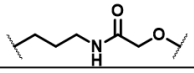	30%

Figure 3. Linker optimization for reversible covalent BTK degraders. Optimization of the linkers of the RC series of BTK degraders and their corresponding % of BTK degradation in MOLM-14 cells (200 nM, 24 h incubation). Note: RC-6 was unstable due to intramolecular cyclization with the Michael acceptor.

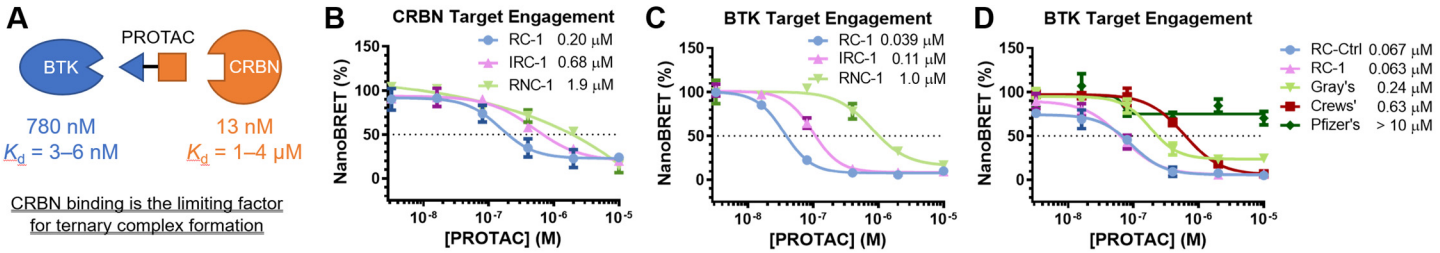

Figure.4. Target engagement for BTK degraders. (A) Quantitative Western blot was performed on lysate of 10^6 MOLM-14 cells using BTK and CRBN recombinant proteins as the standard. Assuming the MOLM-14 volume is 1000 μM^3, we can calculate the BTK and CRBN concentrations are 780 and 13 nM, respectively. Considering the weak binding between pomalidomide and CRBN, we can conclude that CRBN binding is the limiting factor for ternary complex formation. (B) CRBN in-cell target engagement assay. HEK-293 cells were transiently transfected with plasmids expressing a fusion protein of CRBN and nano-luciferase (nLuc) for 24 h and then the cells were treated with a CRBN tracer, which binds to CRBN to induce energy transfer signals. Adding PROTACs to cells would compete the CRBN tracer binding to CRBN, thus reducing the NanoBRET signals. It should be noted that the NanoBRET assay is ratiometric and independent of the expression level of the nLuc fusion protein. The IC_{50} values for RC-1, IRC-1, and RNC-1, defined as concentrations that can reduce normalized BRET signals by 50%, are 0.20, 0.68. and 1.9 μM, respectively. (C) BTK in-cell target engagement assay. This assay is the same as the CRBN in-cell target engagement assay, except BTK-nLuc fusion plasmid and BTK tracer were used. The IC_{50} values for RC-1, IRC-1, and RNC-1 are 0.039, 0.11 and 1.0 μM, respectively. (D) The same BTK in-cell target engagement assay as in (C) was applied to RC-1, RC-Ctrl, Gray's, Crews' and Pfizer's BTK degraders. The target engagement IC_{50} values for RC-1 and RC-Ctrl are the same within experimental errors, demonstrating that the cellular permeability of RC-1 is similar to its parent warhead molecule. In contrast, the target engagement IC_{50} values for Gray's and Crews' BTK degraders are 4 and 10 folds of that of RC-1, respectively. Surprisingly, Pfizer's BTK degrader did not show appreciable target engagement even at 10 μM. Triplicates were performed with SEM as the error bars.

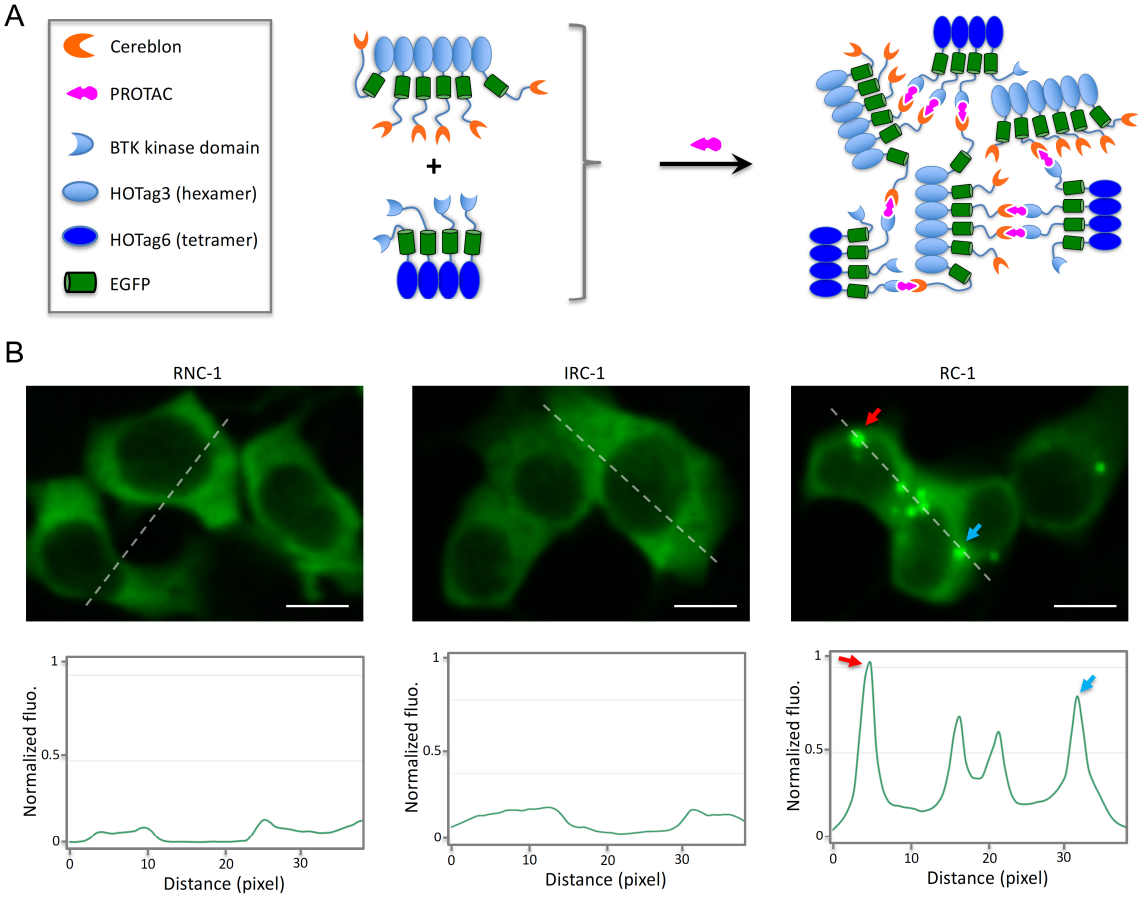

Figure 5. Fluorophore phase separation-based assay for imaging ternary complex formation in living cells. (A). Schematic diagram showing the design of the cellular assay. (B). Fluorescence images showing detection of BTK PROTACs-induced interaction between the E3 ligase cereblon and the target protein BTK. A fluorescence histogram of the line across the cells is shown below. HEK293 cells transiently expressed BTK^{KD}-EGFP-HOTag6 and CRBN-EGFP-HOTag3. RC-1, IRC-1 and RNC-1 (10 μM) were added to the cells. Scale bar: 10 μm. Please contact Dr. Xiaokun Shu (xiaokun.shu@ucsf.edu) for assay details.

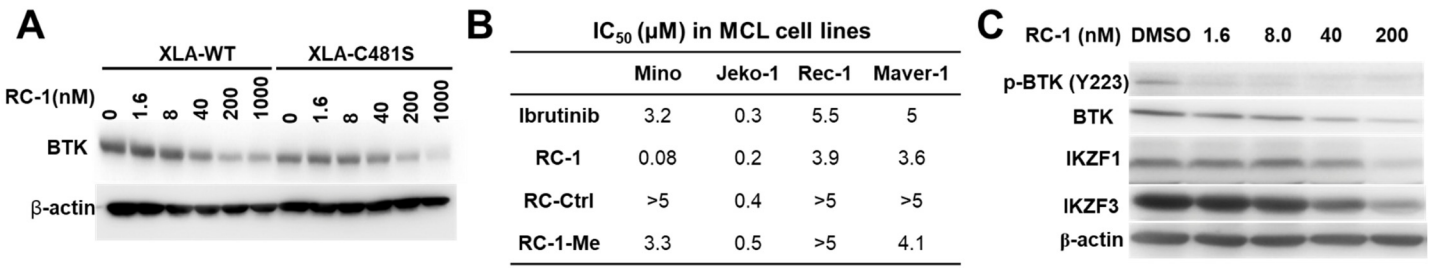

Figure 6. RC-1 overcomes drug resistance. (A) XLA cells overexpressing wild type or C481S mutant BTK were treated with RC-1 for 24 h. Then Western blotting was performed to evaluate the degradation of BTK. Duplicates were performed. (B) IC_{50} values of ibrutinib, RC-1, RC-Ctrl, and RC-1-Me in MCL cell lines. (C) RC-1 induced degradation of BTK, pBTK, IKZF1 and IKZF3 in Mino cells.

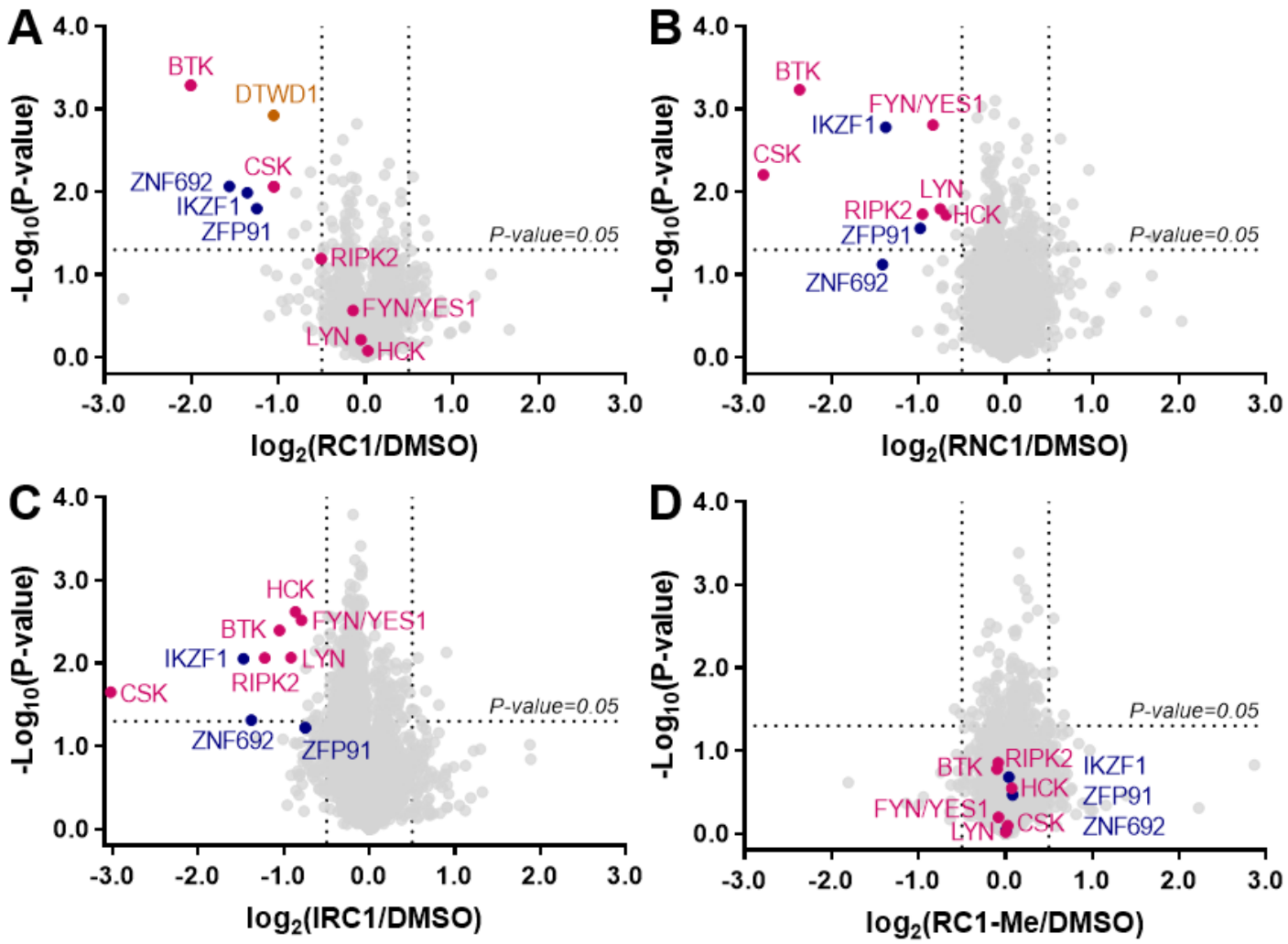

Figure.7. Proteomic analysis showing RC-1 selectively degrades BTK. MOLM-14 cells were treated with either compounds [200 nM (A) RC-1, (B) RNC-1, (C) IRC-1, or (D) RC-1-Me (RC-1 non-degrader control)] or DMSO for 24 h. Lysates were treated with a TMT-10plex kit and subjected to mass spec-based proteomics analysis. Datasets represent an average of duplicates. Volcano plot shows protein abundance (log2) as a function of significance level (log10). Nonaxial vertical lines denote abundance changes from 0.7 to 1.4 (i.e. $2^{\pm 0.5}$), whereas nonaxial horizontal line marks P = 0.05 significance threshold. Downregulated proteins of significance are found in the upper left quadrant of the plots. Violet red dots represent kinases. Dark blue dots represent zinc finger proteins. Both RNC-1 and IRC-1 showed significant degradation of 7 kinases, while RC-1 only degrades BTK and CSK. A total of 7,280 proteins were identified, and only the ones with at least one uniquely identified peptide are displayed.

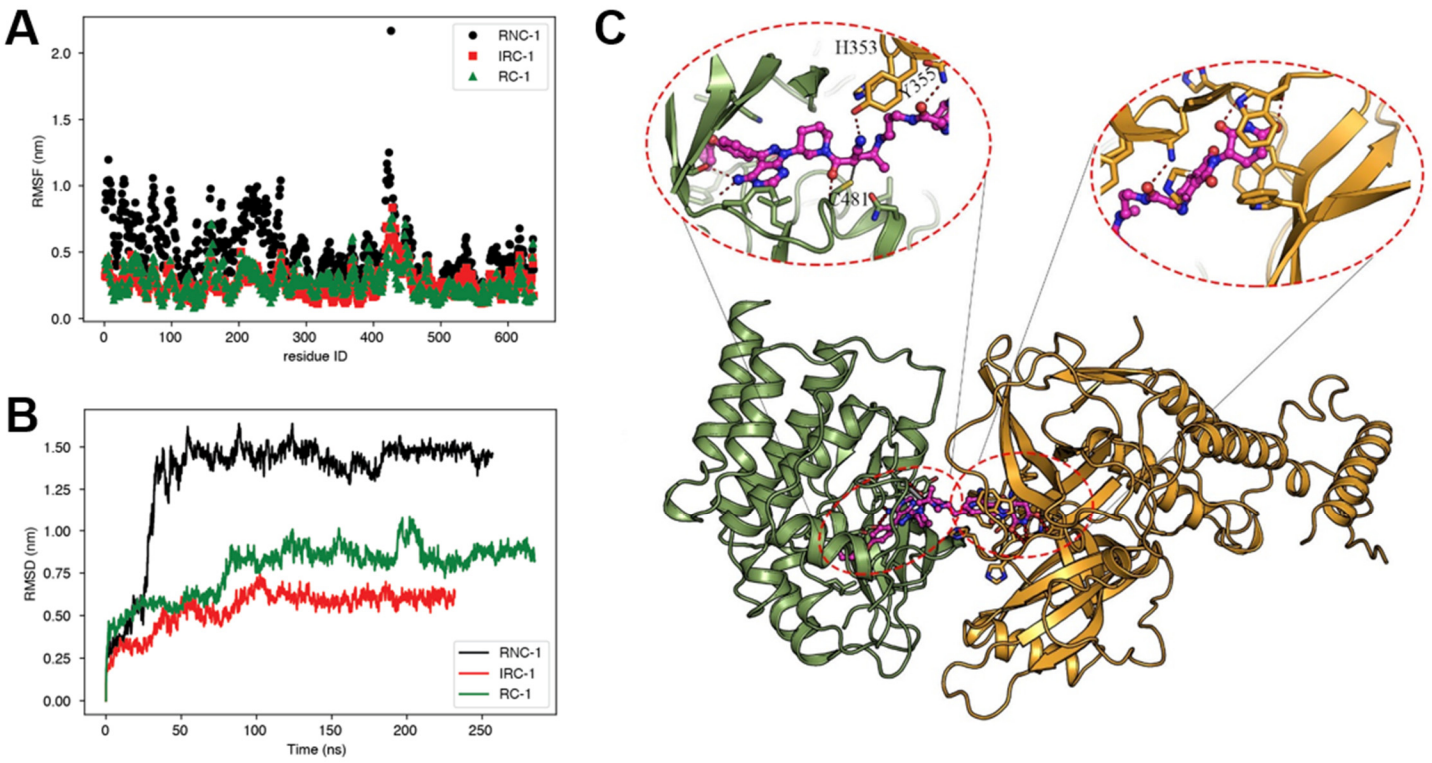

Figure 8. Molecular dynamics simulations for ternary complexes of BTK-PROTAC-CRBN. (A) RNC-1 mediated complex shows a larger structural fluctuation compared with the other two ligands, reflected by (A) Root Mean Square Fluctuation (RMSF) per residue and (B) Root Mean Square Deviation (RMSD) calculated from the simulations of the {BTK-PROTAC-CRBN} ternary complexes. (C) Predicted most stable conformation of {BTK-RC-1-CRBN} ternary complex. Red dashes indicate the hydrogen bonds formed among the ligand, proteins, or waters. Light green cartoons are BTK and cyan cartoons are E3 ligase. Magenta stick ball models represent RC-1.

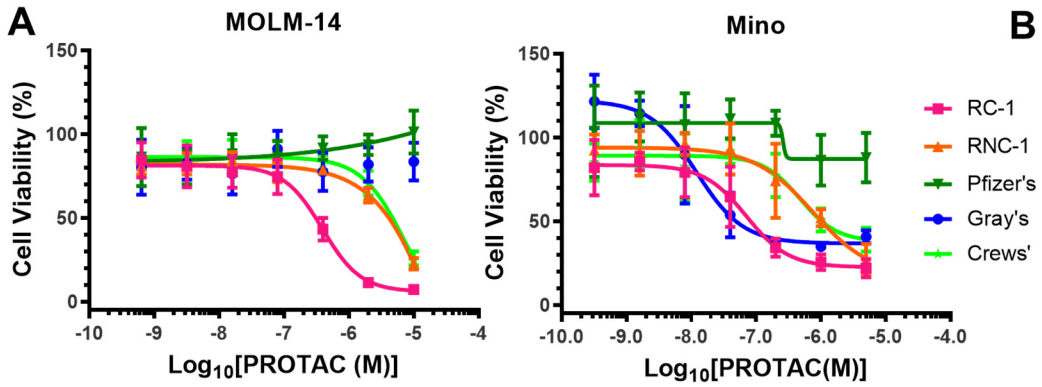

B

IC_{50} (μM) of BTK degraders

Compd.	MOML-14	Mino
RC-1	0.3	0.08
RNC-1	4.1	1.0
Pfizer's	NA	NA
Gray's	NA	0.05
Crews'	4.7	1.0

Figure 9. Comparison of RC-1 with BTK degraders reported. BTK degraders from Pfizer (compound 9), the Gray group (DD-03-171), and the Crews' group (MT-802) were synthesized in house. The cells were treated with compounds for 72 h. Then MTT assays were performed to quantify the cellular viabilities.

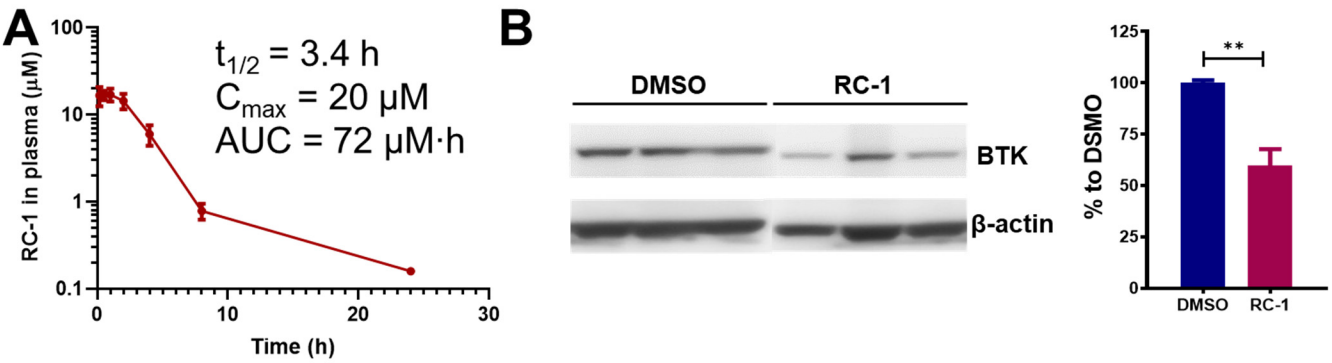

Figure 10. PK/PD of RC-1. (A) RC-1 (20 mg/kg, single i.p. injection) in ICR mice plasma (n=3). (B) Representative western blot (left) and quantification (right) of splenic BTK level in mice (n=3) treated with 7 once daily i.p. injection of 20 mg/kg RC-1 (spleens were harvested 24 h after the 7th injection).

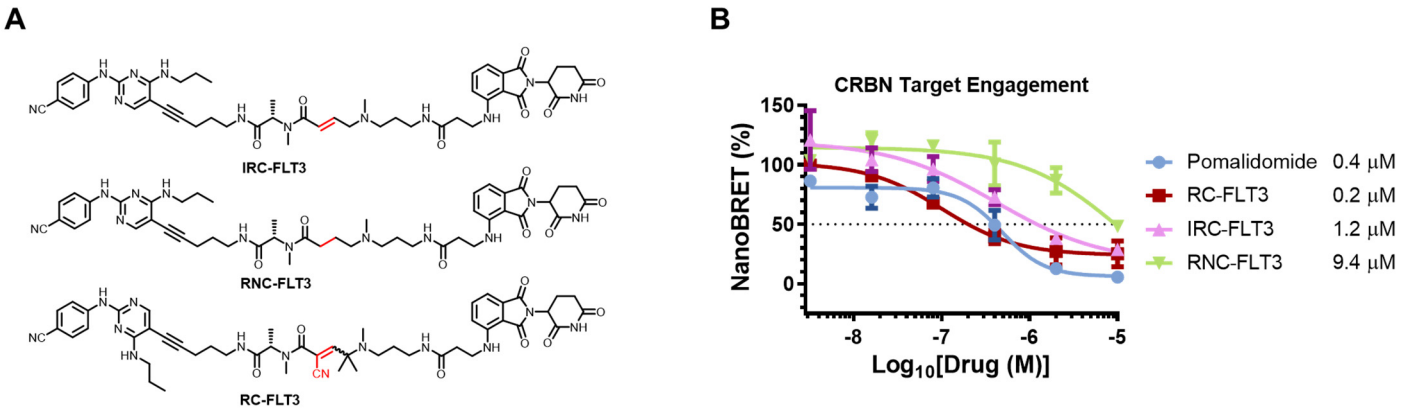

Figure 11. Target engagement for FLT3 degraders. (A) Chemical structures of FLT3 degraders. (B) CRBN in-cell target engagement assay. HEK-293 cells were transiently transfected with plasmids expressing a fusion protein of CRBN and nano-luciferase (nLuc) for 24 h and then the cells were treated with a CRBN tracer, which binds to CRBN to induce energy transfer signals. Adding drugs to cells would compete the CRBN tracer binding to CRBN, thus reducing the NanoBRET signals. The IC_{50} values for Pomalidomide, RC-FLT3, IRC-FLT3 and RNC-FLT3, defined as concentrations that can reduce normalized BRET signals by 50%, are 0.40, 0.20, 1.2 and 9.4 μM, respectively.

References

1. Burslem, G.M. & Crews, C.M. Small-Molecule Modulation of Protein Homeostasis. *Chem Rev* **117**, 11269-11301 (2017).
2. Sakamoto, K.M. et al. Protacs: chimeric molecules that target proteins to the Skp1-Cullin-F box complex for ubiquitination and degradation. *Proc Natl Acad Sci U S A* **98**, 8554-9 (2001).
3. Scudellari, M. Protein-slaying drugs could be the next blockbuster therapies. *Nature* **567**, 298-300 (2019).
4. Bondeson, D.P. et al. Catalytic in vivo protein knockdown by small-molecule PROTACs. *Nat Chem Biol* **11**, 611-7 (2015).
5. Burslem, G.M. et al. The Advantages of Targeted Protein Degradation Over Inhibition: An RTK Case Study. *Cell Chem Biol* **25**, 67-77 e3 (2018).
6. Graves, L.M., Duncan, J.S., Whittle, M.C. & Johnson, G.L. The dynamic nature of the kinome. *Biochem J* **450**, 1-8 (2013).
7. Leiser, D. et al. Targeting of the MET receptor tyrosine kinase by small molecule inhibitors leads to MET accumulation by impairing the receptor downregulation. *FEBS Lett* **588**, 653-8 (2014).
8. Gadd, M.S. et al. Structural basis of PROTAC cooperative recognition for selective protein degradation. *Nat Chem Biol* **13**, 514-521 (2017).
9. Smith, B.E. et al. Differential PROTAC substrate specificity dictated by orientation of recruited E3 ligase. *Nat Commun* **10**, 131 (2019).
10. Jiang, B. et al. Development of Dual and Selective Degraders of Cyclin-Dependent Kinases 4 and 6. *Angew Chem Int Ed Engl* **58**, 6321-6326 (2019).
11. Brand, M. et al. Homolog-Selective Degradation as a Strategy to Probe the Function of CDK6 in AML. *Cell Chem Biol* **26**, 300-306 e9 (2019).
12. Bai, L. et al. A Potent and Selective Small-Molecule Degrader of STAT3 Achieves Complete Tumor Regression In Vivo. *Cancer Cell* **36**, 498-511 e17 (2019).
13. Tinworth, C.P. et al. PROTAC-Mediated Degradation of Bruton's Tyrosine Kinase Is Inhibited by Covalent Binding. *ACS Chem Biol* **14**, 342-347 (2019).
14. Buckley, D.L. et al. HaloPROTACS: Use of Small Molecule PROTACs to Induce Degradation of HaloTag Fusion Proteins. *ACS Chem Biol* **10**, 1831-7 (2015).
15. Jiang, X. et al. Quantitative Real-Time Imaging of Glutathione with Sub-Cellular Resolution. *Antioxid Redox Signal* (2018).
16. Jiang, X. et al. Quantitative real-time imaging of glutathione. *Nat Commun* **8**, 16087 (2017).
17. Jiang, X. et al. Quantitative imaging of glutathione in live cells using a reversible reaction-based ratiometric fluorescent probe. *ACS Chem Biol* **10**, 864-74 (2015).
18. Chen, J. et al. Reversible Reaction-Based Fluorescent Probe for Real-Time Imaging of Glutathione Dynamics in Mitochondria. *ACS Sens* **2**, 1257-1261 (2017).
19. Bradshaw, J.M. et al. Prolonged and tunable residence time using reversible covalent kinase inhibitors. *Nat Chem Biol* **11**, 525-31 (2015).
20. Woyach, J.A. et al. Resistance mechanisms for the Bruton's tyrosine kinase inhibitor ibrutinib. *N Engl J Med* **370**, 2286-94 (2014).
21. Johnson, A.R. et al. Battling Btk Mutants With Noncovalent Inhibitors That Overcome Cys481 and Thr474 Mutations. *ACS Chem Biol* **11**, 2897-2907 (2016).
22. Sun, Y. et al. PROTAC-induced BTK degradation as a novel therapy for mutated BTK C481S induced ibrutinib-resistant B-cell malignancies. *Cell Res* **28**, 779-781 (2018).
23. Huang, H.T. et al. A Chemoproteomic Approach to Query the Degradable Kinome Using a Multi-kinase Degrader. *Cell Chem Biol* **25**, 88-99 e6 (2018).
24. Zorba, A. et al. Delineating the role of cooperativity in the design of potent PROTACs for BTK. *Proc Natl Acad Sci U S A* **115**, E7285-E7292 (2018).
25. Buhimschi, A.D. et al. Targeting the C481S Ibrutinib-Resistance Mutation in Bruton's Tyrosine Kinase Using PROTAC-Mediated Degradation. *Biochemistry* **57**, 3564-3575 (2018).
26. Dobrovolsky, D. et al. Bruton tyrosine kinase degradation as a therapeutic strategy for cancer. *Blood* **133**, 952-961 (2019).
27. Crew, A.P. et al. Identification and Characterization of Von Hippel-Lindau-Recruiting Proteolysis Targeting Chimeras (PROTACs) of TANK-Binding Kinase 1. *J Med Chem* **61**, 583-598 (2018).

28. Brown, G.C. Total cell protein concentration as an evolutionary constraint on the metabolic control distribution in cells. *J Theor Biol* **153**, 195-203 (1991).
29. Douglass, E.F., Jr., Miller, C.J., Sparer, G., Shapiro, H. & Spiegel, D.A. A comprehensive mathematical model for three-body binding equilibria. *J Am Chem Soc* **135**, 6092-9 (2013).
30. Chung, C.I., Zhang, Q. & Shu, X. Dynamic Imaging of Small Molecule Induced Protein-Protein Interactions in Living Cells with a Fluorophore Phase Transition Based Approach. *Anal Chem* **90**, 14287-14293 (2018).
31. Riching, K.M. et al. Quantitative Live-Cell Kinetic Degradation and Mechanistic Profiling of PROTAC Mode of Action. *ACS Chem Biol* **13**, 2758-2770 (2018).
32. Gasparini, G., Sargsyan, G., Bang, E.K., Sakai, N. & Matile, S. Ring Tension Applied to Thiol-Mediated Cellular Uptake. *Angew Chem Int Ed Engl* **54**, 7328-31 (2015).
33. Abegg, D. et al. Strained Cyclic Disulfides Enable Cellular Uptake by Reacting with the Transferrin Receptor. *J Am Chem Soc* **139**, 231-238 (2017).
34. Zhang, Y., Huo, M., Zhou, J. & Xie, S. PKSolver: An add-in program for pharmacokinetic and pharmacodynamic data analysis in Microsoft Excel. *Comput Methods Programs Biomed* **99**, 306-14 (2010).
35. Yamaura, T. et al. A novel irreversible FLT3 inhibitor, FF-10101, shows excellent efficacy against AML cells with FLT3 mutations. *Blood* **131**, 426-438 (2018).
36. Krishnan, S. et al. Design of reversible, cysteine-targeted Michael acceptors guided by kinetic and computational analysis. *J Am Chem Soc* **136**, 12624-30 (2014).
37. Saito, K. et al. BTK regulates PtdIns-4,5-P2 synthesis: importance for calcium signaling and PI3K activity. *Immunity* **19**, 669-78 (2003).
38. Middendorp, S., Dingjan, G.M., Maas, A., Dahlenborg, K. & Hendriks, R.W. Function of Bruton's tyrosine kinase during B cell development is partially independent of its catalytic activity. *J Immunol* **171**, 5988-96 (2003).
39. Nyhoff, L.E. et al. Bruton's Tyrosine Kinase Is Not Essential for B Cell Survival beyond Early Developmental Stages. *J Immunol* **200**, 2352-2361 (2018).
40. Ronen, G. et al. *Efficient targeted degradation via reversible and irreversible covalent PROTACs*, (2020).